DNA-based fluorescent probes of NOS2 activity in live brains

Aneesh T Veetil[1,2], Junyi Zou [#1,2], Katharine W Henderson [#3], Maulik S Jani [#1,2], Shabana Mehtab[3,4], Sangram S. Sisodia[3,4], Melina E. Hale [2,3] and Yamuna Krishnan[1,2]

1. *Department of Chemistry, University of Chicago, Chicago, IL, 60637, USA*
2. *Grossman Institute of Neuroscience, Quantitative Biology and Human Behavior, University of Chicago, Chicago, IL, 60637, USA*
3. Department of Organismal Biology and Anatomy, The University of Chicago, 1027 E. 57th Street, Chicago, IL 60637, USA.
3. *Department of Neurobiology, University of Chicago, Chicago, IL, 60637, USA*
4. *The Microbiome Center, University of Chicago, Chicago, IL, 60637, USA.*

*# Equal contribution, *Correspondence to: yamuna@uchicago.edu*

Entry	Sequence
S1-strand	5'-DAR-PEG10/ATCAACACTGCACACCAGACAGCA-3'
S2-strand	5'-ATTO647N/TGCTGTCTGGTGTGCAGTGTTGAT-3'
NOckout^{1826CpG}	5'-ATTO647N/TGCTGTCTGGTGTGCAGTGTTGATtttccatgacgttcctgacgtt-3' 3'-ACGACAGACCACACGTCACAACTA/PEG10-DAR-5'
NOckout^{1826GC}	5'-ATTO647N/TGCTGTCTGGTGTGCAGTGTTGATtttccatgagcttcctgagctt-3' 3'-ACGACAGACCACACGTCACAACTA/PEG10-DAR-5'
NOckout^{2007CpG}	5'-ATTO647N/TGCTGTCTGGTGTGCAGTGTTGATtttcgtcgttgtcgttttgtcgtt-3' 3'-ACGACAGACCACACGTCACAACTA/PEG10-DAR-5'
NOckout^{2007GC}	5'-ATTO647N/TGCTGTCTGGTGTGCAGTGTTGATtttgctgcttgtgcttttgtgctt-3' 3'-ACGACAGACCACACGTCACAACTA/PEG10-DAR-5'
NOckout^{iRNA}	5'-ATTO647N/TGCTGTCTGGTGTGCAGTGTTGATtttggacggaaagaccccgugg-3' 3'-ACGACAGACCACACGTCACAACTA/PEG10-DAR-5'
NOckout^{RNA}	5'-ATTO647N/TGCTGTCTGGTGTGCAGTGTTGATtttggacgggaagaccccgugg-3' 3'-ACGACAGACCACACGTCACAACTA/PEG10-DAR-5'
NOckout^{UN}	5'-ATTO647N/TGCTGTCTGGTGTGCAGTGTTGAT-3' 3'-ACGACAGACCACACGTCACAACTA-5'
pHlava-SH	5'-HS-ATCAACACTGCACACCAGACAGCA-3'

Supplementary Table 1: Table shows sequences of oligonucleotides with chemical modifications used in this study. Small alphabets at the 3'-end represent either CpG or ORN sequences with phosphorothioate modifications.

www.pnas.org/cgi/doi/10.1073/pnas.2003034117

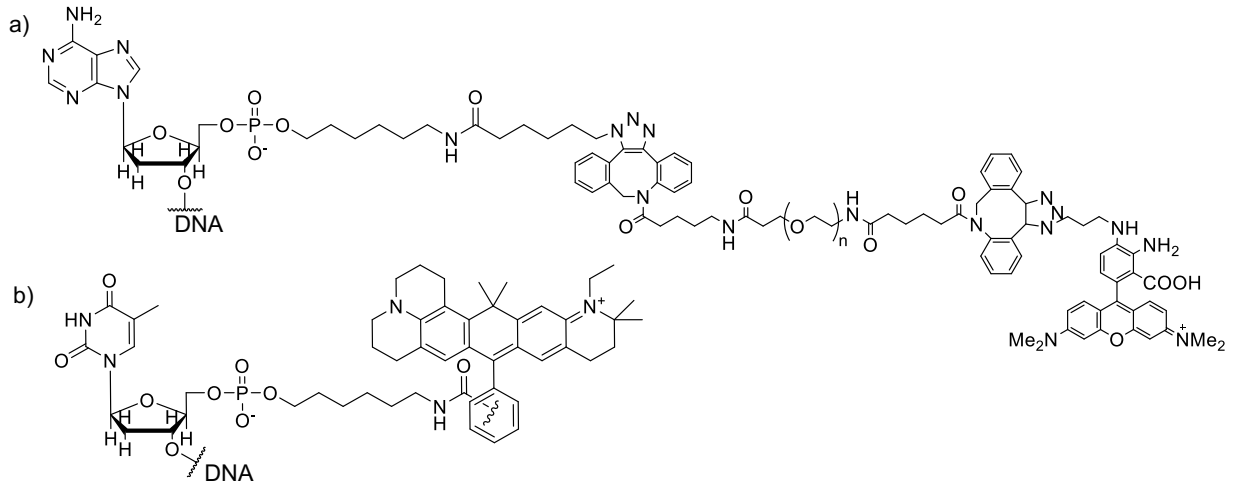

Supplementary Scheme 1: (a) Chemical structure of DAR, linked to the ssDNA (24-mer) to its 5'-end using a long polyethylene glycol linker. (b) Chemical structure of ATTO647N fluorophore (normalizing dye) linked to the 5'-end of fully complementary ssDNA (24-mer).

Stepwise assembly of *NOckout* sensors

Step 1. Synthesis of bifunctional PEG conjugate DBCO-PEG-NH-BOC: 10 kDa polyethylene glycol linker (3mg, 0.0003 mmol) was dissolved in 150 µL freshly dry DMSO. 2 µL of extra dry trimethylamine (TEA) was added to the above solution to maintain a pH ~ 8.0 and the mixed by constant stirring. To that mixture, DBCO-NHS (20 mM, cat no # 761524, Sigma) ester dissolved in dry DMSO (50 µL) was added. The reaction mixture was stirred at room temperature for ~3 hours and subsequently the mixture was diluted by adding of excess of (100x) milli-Q water to bring down the DMSO content in the mixture less than 1% (w/v). The clear reaction mixture was then loaded to an Amicon ultra centrifugation filter (MWCO ~ 3 kDa, Merck Millipore) to remove excess of DBCO-NHS ester by spinning at 12000 rpm for 10 min at 4 ºC. The centrifugation step was repeated using milli-Q water until no trace of DBCO-NHS was detected in the filtrate using UV-Vis spectroscopy (λ_{ab} = 309 nm, ε = 12000 $M^{-1}cm^{-1}$). The product was subsequently lyophilized to obtain a white fluffy powder and it was stored at -80°C for up to 6 months.

Step 2. Deprotection of DBCO-PEG-NH-BOC: Removal of *tert*-butyloxycarbonyl (t-Boc) group in DBCO-PEG-NH-BOC (2 mg) was achieved by dissolving it an Eppendorf tube (1.5 ml) containing 200 µL mixture of trifluoroacetic acid/dichloromethane (5:95 v/v). The mixture was stirred overnight at room temperature. Subsequently, the solvent mixture was evaporated by using a gentle nitrogen flow. 100 µL milli-Q water was added to the residue and followed by this trimethylamine (TEA) was added till the pH of the solution reached 7.0. The solution was further centrifuged with milli-Q water using a MWCO ~ 3 kDa filter to remove excess TEA. The product was quantified by UV-Vis spectroscopy using DBCO absorption (λ_{ab} = 309 nm, ε = 12000 $M^{-1}cm^{-1}$) and subsequently lyophilized to store at -80°C for up to 6 months.

Step 3. DNA-PEG conjugation: A 24-mer ssDNA containing 5'-azido group (Supplementary table T1) was dissolved in 50 mM potassium phosphate buffer pH 7.4 to a final concentration of 50 µM.

DBCO-PEG-NH_2 (60 μM) was added to the ssDNA solution and the reaction mixture was stirred overnight. Completion of the click reaction was monitored by using a 15 % native PAGE gel shift assay (SI Figure 2). Purification of the reaction mixture was performed by using a 10 kDa MWCO Amicon ultra centrifugal filter tubes (2 mL, Merck Millipore) using phosphate buffer (pH 7.4) as an eluent. The attachment of PEG to the ssDNA was confirmed from the retarded mobility of ssDNA-PEG-NH2 conjugate compared to the ssDNA on the native polyacrylamide gel (15%) (SI Figure 3a).

Step 3. Synthesis of ssDNA-PEG-DBCO: Capping of the terminal -NH_2 group in ssDNA-PEG-NH_2 (45 μM, dissolved in phosphate buffer, pH 7.4) with a DBCO group was achieved by reacting it with DBCO-NHS (20 mM, Cat No # 761524, Sigma) dissolved in DMSO. The mixture was let to stir for 3 hours at room temperature and excess of DBCO-NHS was subsequently removed by using a 3 kDa Amicon filter as described above. Pure product obtained after centrifugation was quantified by using UV-Vis spectroscopy using DBCO absorbance (λ_{ab} = 309 nm, ε = 12000 $M^{-1}cm^{-1}$) and was stored at -80°C. See SI Figure 3a for gel characterization of the product.

Step 4. Synthesis of ssDNA-PEG-DAR: An aliquot of 3.33 μL (3 mM) of DAR-N_3 in DMSO was mixed with 50 μM of ssDNA-PEG-DBCO in 100 μL of phosphate buffer (pH 7.4, 50 mM). The reaction was stirred overnight at room temperature to achieve a 1:1 labeling of ssDNA with the DAR-N_3. The crude reaction mixture was centrifuged multiple rounds (12000 rpm for 10 min at 4 ºC) to remove unreacted DAR-N_3 till no trace of it was detected in the filtrate (λ_{em} = 571 nm, ε = 7.8 x 104 $M^{-1}cm^{-1}$). A ratio of 1:1 labeling of the DAR to the DNA was confirmed by using UV-Vis spectroscopy (SI Figure 2). See Figure 3a for gel characterization of the product.

NOckout **and** ***NOckout^{Fn}*** **synthesis**: *NOckout* was assembled by annealing 24-mer ssDNA-PEG-DAR (20 μM) with a 24-mer 5'-ATTO647N labeled complementary ssDNA (20 μM) in phosphate or HBSS buffer (50 mM, pH 7.2). The individual ssDNA samples were mixed together and the mixture was subsequently annealed from 70 ºC to room temperature by applying a temperature gradient of 5 ºC/15 minutes using ThermoMixer C (Eppendorf). The annealed sample was further incubated at 4 ºC for 2 hours. The formation of *NOckout* was verified using native polyacrylamide gel electrophoresis (15%) as shown in SI figure 3. We have used six functionally different *NOckout^{Fn}* probes in this study (see Figure 1a). All these probes were synthesized by using a similar protocol that was described above for *NOckout* assembly by using different complementary ssDNA strand carrying A647N fluorophore (e.g. mCpG sequence, SI table 1). 24-mer ssDNA-PEG-DAR (20 μM) DNA was annealed with corresponding 24-mer functional A647N strand (20 μM) in pH 7.2 phosphate buffer. Self-assembly and integrity of the probes (SI Figure 3b-e) were checked using native PAGE as described below.

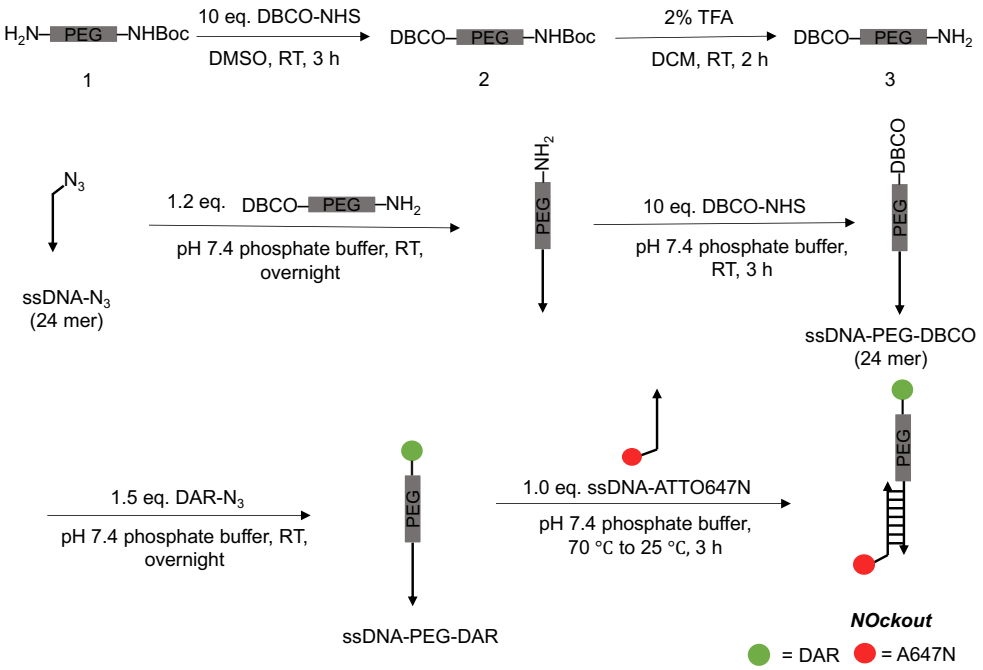

Supplementary Figure 1: Bio-conjugation steps employed in the synthesis of *NOckout* probe. A 10 kDa bifunctional PEG linker was employed to chemically link DAR-fluorophore to the ssDNA to obtain ssDNA-PEG-DAR, which was then annealed to an ssDNA-ATTO647N strand to assemble *NOckout*. Green circle represents DAR-fluorophore and red-circle represents ATTO647N, the normalizing fluorophore.

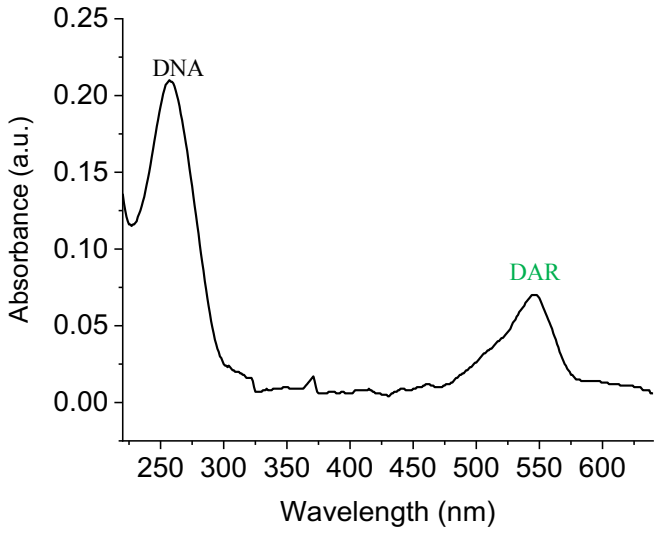

Supplementary Figure 2: UV-Vis absorption spectrum of ssDNA-PEG-DAR (0.8 μM, in 100 mM phosphate buffer, pH 7.2 at 25°C) showing a 1:1 labeling of NO-sensing fluorophore (DAR) to the 24-mer ssDNA-strand.

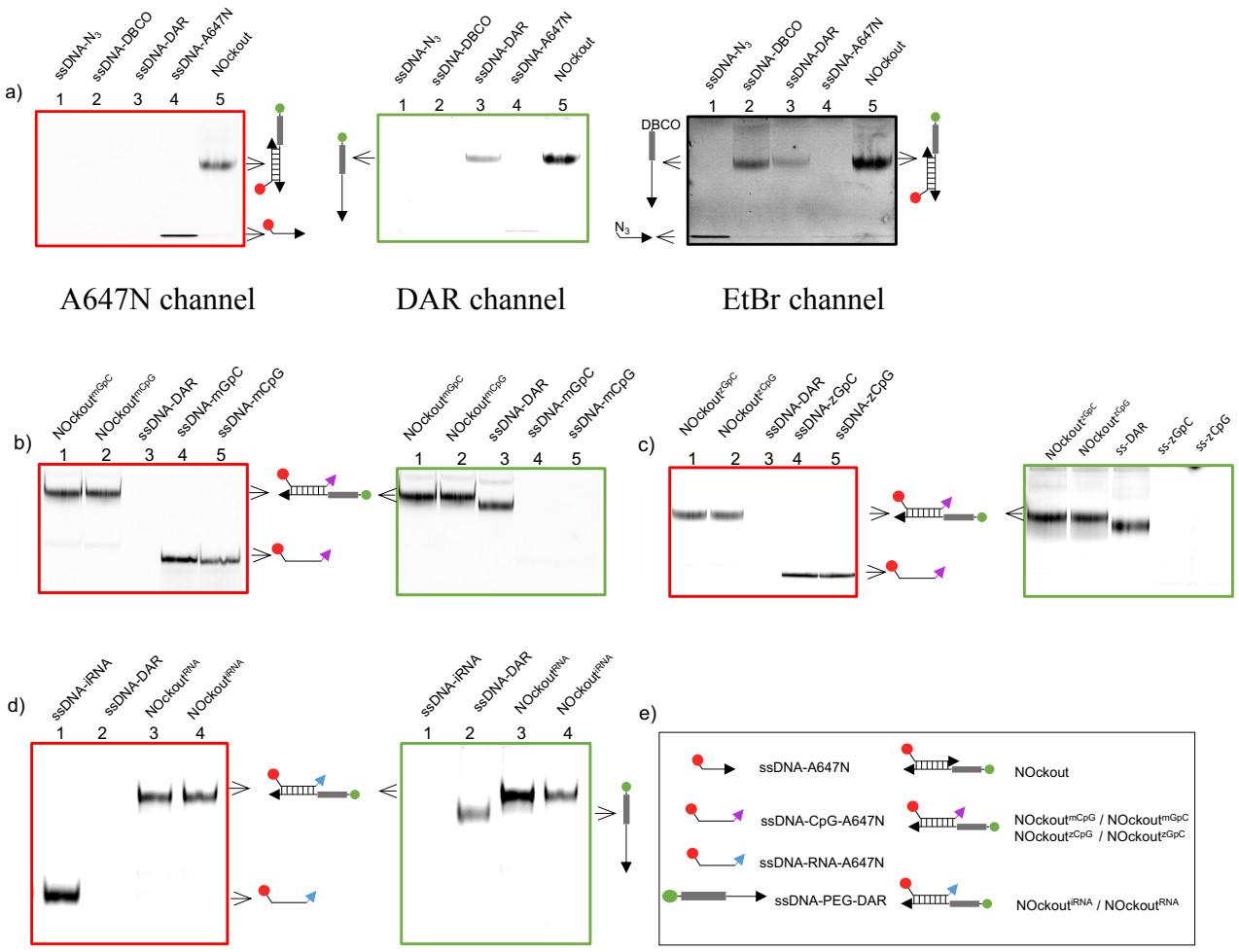

Supplementary Figure 3: Characterization of *NOckout* probes using gel electrophoresis. (a) Gel mobility shift observed for *NOckout* in a 15% native polyacrylamide gel excited in the A647N (red box), DAR (green box) and EtBr channels (black box). Panels (b), (c) and (d) shows mobility of $NOckout^{mCpG}$, $NOckout^{zCpG}$ and $NOckout^{iRNA}$ respectively in 15% PAGE. (e) Cartoons representing all the DNA and RNA conjugates used in the gel shift assay.

pH sensitivity of *NOckout* probes: pH insensitivity of *NOckout* probes are critical for error-free reporting of NO from acidic intracellular compartments. We have validated that all the seven *NOckout* probes synthesized were pH insensitive in the range of pH 5- pH 7.4 (SI Figure 4). Briefly, *NOckout* (100 nM in 100 µL) was reacted with 50 µM DEANONOate in pH 6 phosphate buffer (50 mM) to reach the maximum fluorescence in the DAR channel. *NOckout* was subsequently purified using a 3 kDa MWCO Amicon filter by using ultra-centrifugation (12000, rpm, 4 ºC). *NOckout* samples (100 nM) were aliquoted to three different 100 µL microfuge tube containing acetate buffer (pH 5.0, 100 mM), phosphate buffer (pH 6.0, 100 mM) and phosphate buffer (pH 7.4, 100 nM) to a final volume of 100 µL. The samples were incubated for 10 minutes at room temperature to equilibrate and subsequently fluorescence spectra were recorded in DAR (G) and A647N (R) channels. The G/R ratio were calculated and it was found to be independent of pH fluctuations (SI Figure 4).

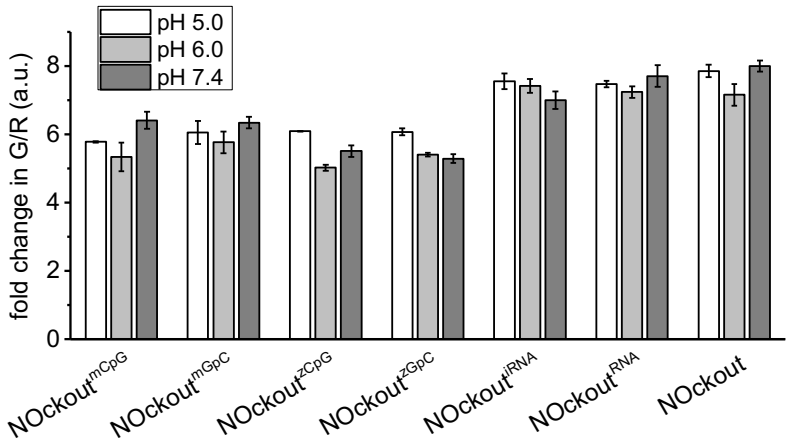

Supplementary Figure 4: Effect of pH on fold change of *NOckout* probes. A647N (R) and DAR (G) fluorophores were excited sequentially at 650 nm and 550 nm respectively and the emission maxima at 660 nm (A647N) and 575 nm (DAR) was computed to obtain the G/R ratio for all the *NOckout* probes. Fold change was represented as the G/R ratio.

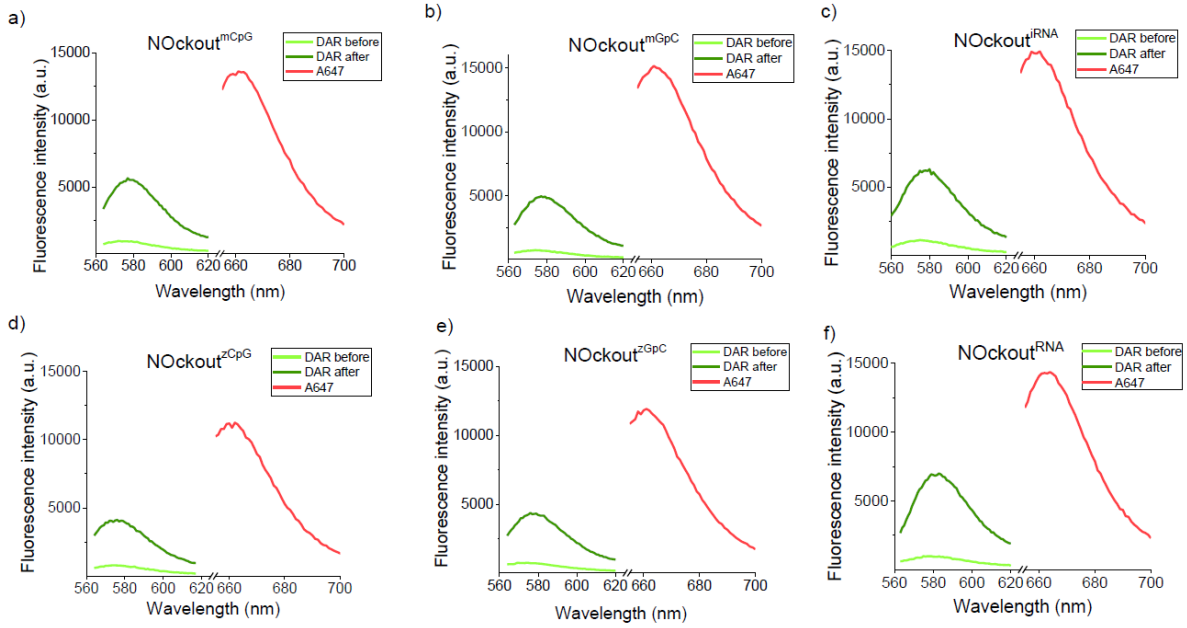

Supplementary Figure 5: Fluorescence emission spectra of *NOckout*^{fn} probes (100 nM) excited in the DAR (λ_{ex} = 550 nm) and A647N (λ_{ex} = 650 nm) channels (slit width = 2 nm each). Light green spectra indicate DAR emission before the addition of NO donor (30 μM) in 50 mM of pH 6.0 phosphate buffer and the dark green spectra represents completely NO reacted DAR at t = 3 minutes. Red curves indicate the emission of A647N that is insensitive to the addition of NO.

Synthesis of *pHlava*: pH sensor *pHlava* is a 24-mer dsDNA duplex carrying a pH sensing fluorophore pHrodo (λ_{ex} = 540 nm, λ_{em} = 580 nm) at the 5'-end of one of the ssDNA strands and

ATTO647N fluorophore on the 5'-end of the complementary ssDNA (see Table S1 for the DNA sequences). pHrodo was attached to the ssDNA using a standard thiol-maleimide conjugation reaction. Briefly, 200 µL of 50 µM ssDNA (in 50 mM phosphate buffer, pH 7.4) carrying a thiol modification at the 5'-terminal was mixed with 200 µM of pHrodo maleimide (2.8 µL from a 14 mM stock in dry DMSO). The reaction mixture was stirred at room temperature for 3 hours and subsequently diluted to final volume of 1 mL using milli-Q water. This solution was then centrifuged using a 3 kDa MWCO ultracentrifugation filter to remove unreacted pHrodo-maleimide. The presence of pHrodo in the filtrate was negated by using UV-Vis spectroscopy (λ_{ab} = 560 nm, ε = 65,000). The ratio of ssDNA to the conjugated pHrodo was confirmed to be 1:1 before proceeding to the annealing step. Annealing of 20 µM ssDNA-pHrodo (in 50 mM of phosphate buffer, pH 7.2) with 20 µM of ssDNA-ATTO647N strand was carried in a ThermoMixer (Eppendorf) at 70 ºC to room temperature by applying a temperature drop of 5 ºC/15 minutes. The annealed sample was further cooled at room temperature and *pHlava* formation was verified using 15% polyacrylamide gel electrophoresis (SI figure S6). The yield of *pHlava* assembly was found to be quantitative.

pH sensitivity of *pHlava* was tested using 200 nM sample in acetate buffer (pH 4.5), phosphate buffer (pH 6.0) and phosphate buffer (pH 7.4) as shown in in SI figure S6. A 3.5-fold decrease in fluorescence intensity was observed in the pHrodo emission maxima (λ_{em}=580 nm) corresponding to a pH decrease from 7.4 to 4.5. The fold change of *pHlava* was calculated as ratio of fluorescence intensity observed for pHrodo at 580 nm to that of the fluorescence intensity of ATTO647N at 660 nm and is shown in SI figure S6.

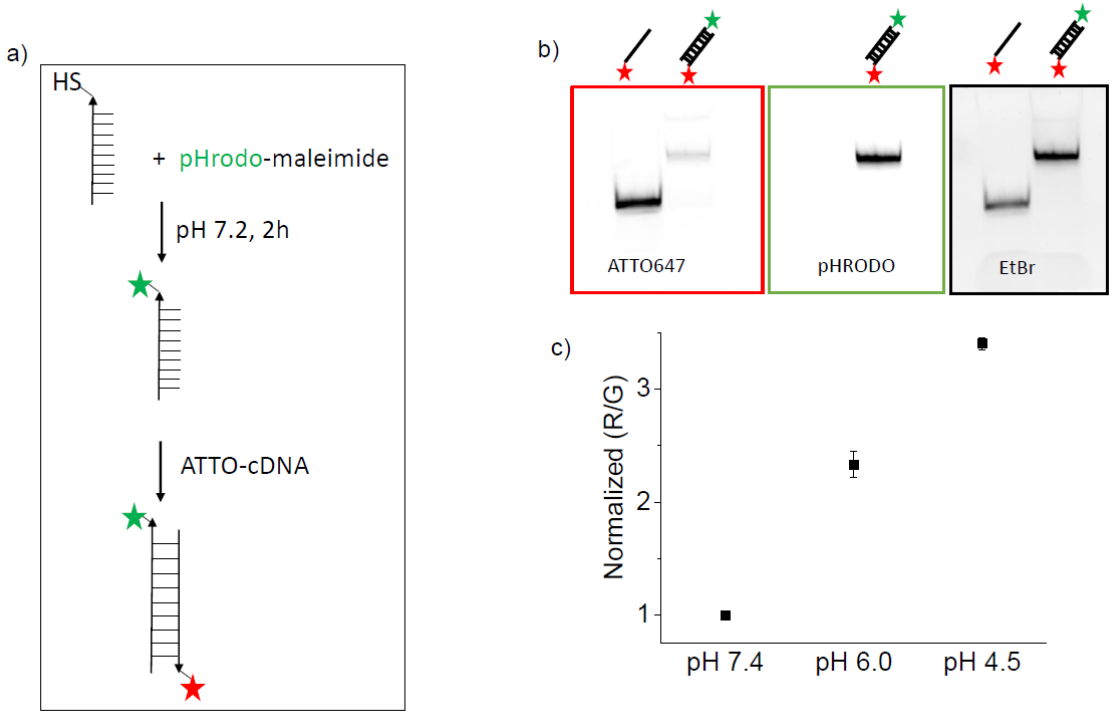

Supplementary Figure 6: Assembly, characterization and pH sensitivity of *pHlava*. (a) Scheme showing the assembly of *pHlava* from a 24-mer thiol (-SH) labeled ssDNA (see SI table1) that is conjugated to *pHrodo*-maleimide. ssDNA conjugated to the *pHrodo* fluorophore was annealed

with fully complementary A647N labeled ssDNA (24-mer) to obtain *pHlava*. (b) 15% PAGE showing the quantitative assembly of *pHlava* and (c) pH sensing property of *pHlava* (200 nM) incubated in respective buffers (see methods) and fluorescence spectra was recorded in the *pHrodo* (Green, G) and A647N channels (Red, R) by exciting at 560 nm and 650 nm respectively. G/R ratio at different pH was calculated and plotted.

Neonatal primary microglia isolation: Mouse primary mixed cortical and hippocampal glial culture were isolated and cultured as described previously[1]. Briefly, brains from postnatal day 1-2 C57BL/6 mice were isolated. After removing of striatum and meninges, the remaining cortical and hippocampal tissue was mechanically dissociated and enzymatically digested in trypsin (Gibco, USA, 59418C) and DNAse-I (10 mg/mL, Sigma, USA, D5025) in HBSS for 30 minutes at 37°C. 1:1 (v/v) Dulbecco's modified Eagle's medium (DMEM, Gibco, USA, 11965092) with 10% fetal bovine serum (FBS, Gibco, USA, 26140079) was added to terminate digestion. Tissue was harvested by centrifugation and plated at a density of 5×10^5 cells/mL in T-75 cm^2 tissue culture flasks. Media was changed the next day and every 3 days until a cellular monolayer had formed after 2 weeks.

Microglia cells were isolated from mixed glial culture after overnight serum-starvation using mild trypsinization as previously described[2]. Media was removed from established mixed glial culture. Cell monolayers were washed with Dulbecco's phosphate buffered saline (DPBS, Gibco, USA, 14040133) to remove residual FBS. Trypsin-EDTA (Gibco, USA, 25200056) diluted 1:4 (v/v) in DMEM was added for mid trypsinization for 45 minutes at 37°C. Detached astrocytic cells were removed and adherent microglia was washed with DPBS followed by supplement of DMEM containing 10% FBS. Isolated microglia cultures were sequentially serum-starved from 10% to 5% to 2.5 % to 0% FBS concentration via daily media changes. Purity of microglia cultures was assessed before experiments (SI Figure 7).

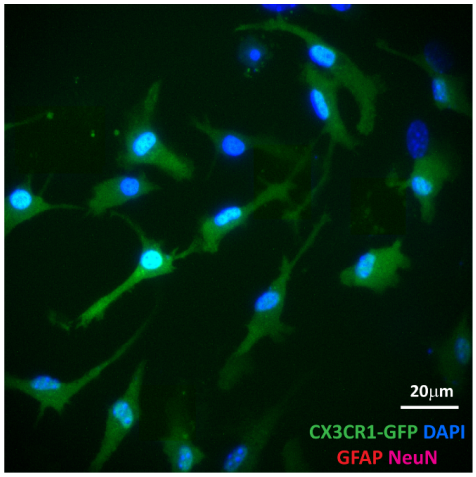

Supplementary Figure 7: Purity of microglial culture. Immunohistochemistry performed on mixed glial culture after the purification process. Astrocytes (red, GFAP maker) and neurons (magenta, NeuN marker) were absent in the culture containing predominantly microglia (green, GFP)

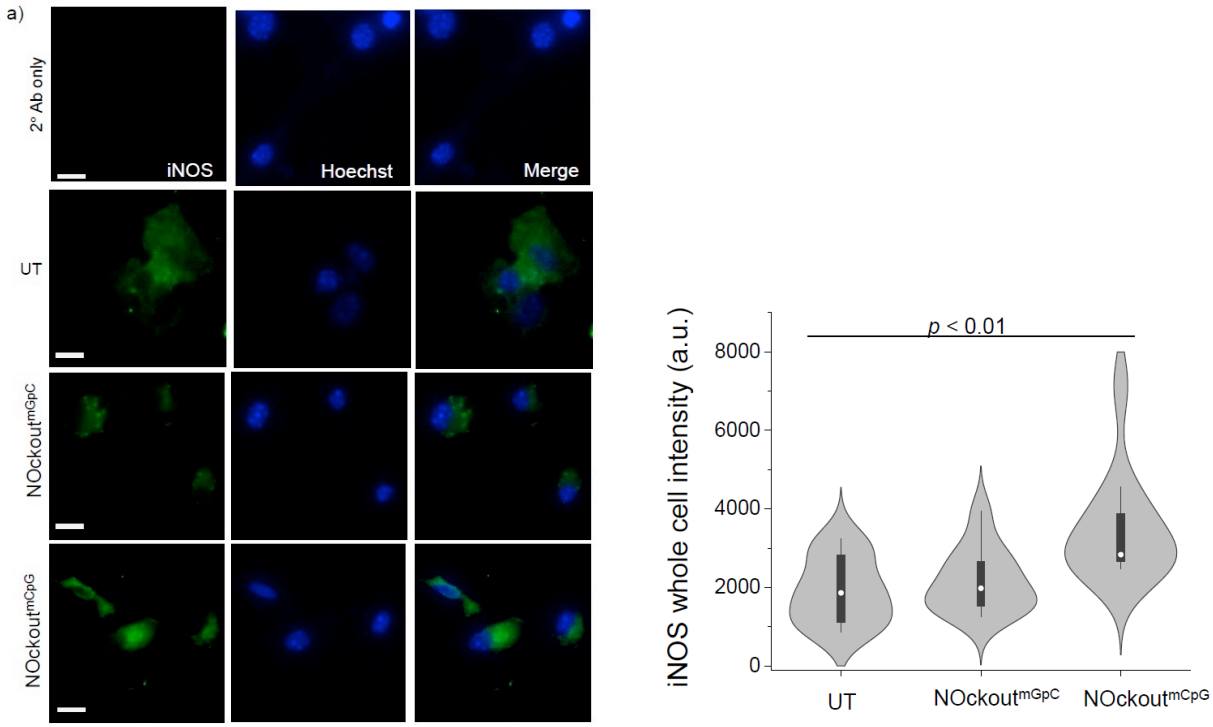

Supplementary Figure 8: iNOS expression in murine primary microglia 2 weeks in culture. (a) Cells were treated with either 1μM *NOckout*^{mCpG} or 1μM *NOckout*^{mGpC} for 3h before fixing with 2.5% paraformaldehyde and subsequently incubated with iNOS antibody (1:30 dilution). A488 (Green) labeled goat anti-rabbit antibody was used for fluorescence detection. (b) Distribution of whole cell iNOS signal obtained for n = 30 cells treated with *NOckout*^{mCpG} and *NOckout*^{mGpC}. Scale bar = 10 μm. p value is obtained by using Kruskal-Wallis statistical test. White circle represents the median G/R value and black bar represents the distribution from 25%–75%.

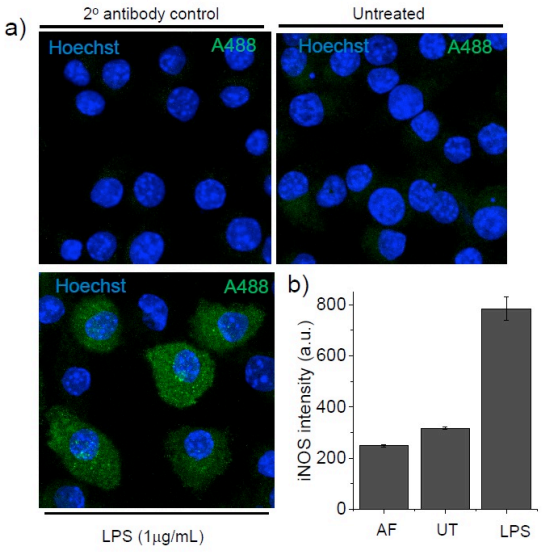

Supplementary Figure 9: iNOS expression in J774A.1 cells. (a) Immunostaining of iNOS in J774A.1 cells, treated with secondary antibody, HBSS (untreated) and LPS (1 µg/ml) (λ_{ex} = 488 nm, green, A488 iNOS antibody) (b) Quantification of whole cell iNOS (green channel) intensities for n = 75 cells. Error bars represent S.E.M from three independent experiments. Hoechst (λ_{ex} = 405 nm, blue) was used as nuclear stain, Scale = 10 µm.

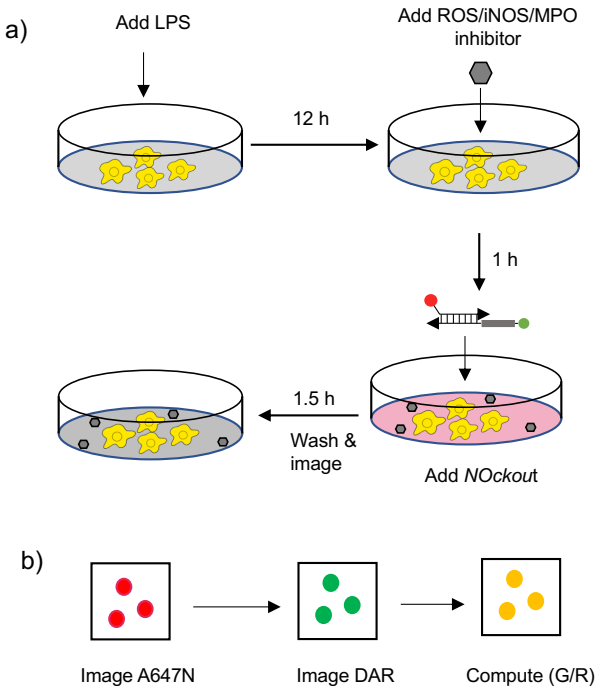

Supplementary Figure 10: (a) Cartoon representing the sequence of *in cellulo* specificity experiment performed in J774A.1 cells with *NOckout* sensor. (b) Fluorescence images from cells were acquired simultaneously in the A647N (red) and DAR (green) channels to compute endosomal G/R ratio (yellow) that represents NO production in those compartments.

***In vitro* specificity of *NOckout* to NO**: *In vitro* specificity experiment of *NOckout* was performed in the presence of NO$^{\bullet}$ and various ROS ($O_2^{\bullet-}$, H_2O_2, HOCl etc.). NO$^{\bullet}$ was generated from corresponding NO$^{\bullet}$ donor, DEANONOate (50 µM). H_2O_2 (100 µM) was used directly from its aqueous stock solution and it was quantified by using UV-Vis spectroscopy ($\varepsilon = 43.6\ M^{-1}cm^{-1}$ at 240 nm). Xanthine/Xanthine oxidase was used for superoxide generation and it was quantified using *Cytochrome* C reduction as described earlier[3]. Hydroxyl radical ($^{\bullet}$OH, 100 µM) was generated using Fenton chemistry of H_2O_2. NaOCl (5 µM) used directly as received (Sigma). Aqueous solutions of NO_2^- and NO_3^- (100 µM) were prepared from their respective sodium salts. *NOckout* (100 nM, pH 6, 50 mM phosphate buffer) was allowed to react with individual ROS and RNS at 37^{o}C for 15 minutes and fluorescent spectra was recorded by exciting DAR (G) and A647N (R) fluorophores. The sensitivity of *NOckout* against different reactive species were expressed as G/R value, where a high G/R indicate high reactivity.

***In cellulo* specificity of *NOckout* to NO**: *In cellulo* specificity of the *NOckout* probe towards NO$^{\bullet}$ was validated in J774A.1 cells. We chose J774A.1 cells due to the known expression of iNOS,

NADPH-oxidase and MPO in those cells and they are also known to produce NO•, $O_2^{\bullet-}$ and HOCl respectively[4,5]. J774A.1 cells were treated with 1 μg/mL LPS for 12 h prior to the addition of *NOckout* (500 nM in HBSS) either in the presence or in absence of specific inhibitors. LPS addition was employed to induce the expression of iNOS, NOX and MPO. This would induce the production of NO• and ROS in the same cells, thus allowing to probe their reactivity towards *NOckout* by using a single and a robust assay. Pharmacological inhibitors of NOX (VAS2870,10 µM), MPO (ABAH, 50 µM) and iNOS (1400W, 10 µM) were added to the media 1 hour before the addition of 500 nM of *NOckout* to J774A.1 cells. After 90 minutes of incubation with the *NOckout*, culture media was removed from the cells and three washes were performed using HBSS to remove extracellular *NOckout* before proceeding to the fluorescence imaging. Inhibitors were present during all the washing steps and in the imaging solution (HBSS). Cells were imaged in live at room temperature using confocal microscopy as described above.

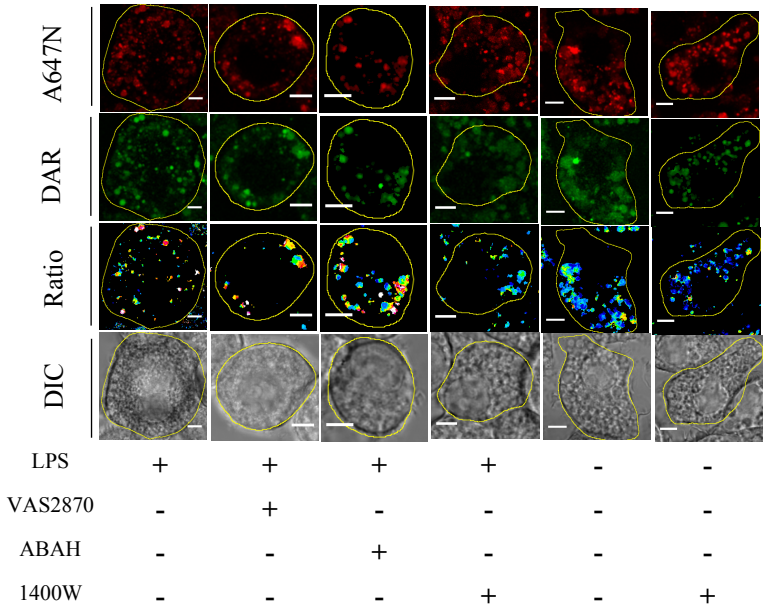

Supplementary Figure 11: *In cellulo* specificity of *NOckout* towards NO in J774 cells. Pharmacological inhibition of NOX using VAS2870 and MPO using ABAH did not reduce NO signal whereas treatment with 1400W (iNOS) inhibitor significantly reduced NO signal. Red represents signal from A647N and green represents DAR signal. Ratio images in heat map represents endosomal G/R values. Scale = 10 µm.

In cellulo* stability of *NOckout: *NOckout* (500 nM in pH 6 phosphate buffer) was treated with DEANONOate (50 µM) until reaching a maximum G/R value as validated by performing *in vitro* fluorescence measurements. J774A.1 cells pretreated with LPS (1 μg/mL) for 12 h and untreated J774A.1 cells were incubated with 500 nM of *NOckout* in HBSS for 30 min. Excess *NOckout* was washed two times with HBSS solution and subsequently complete DMEM was added to the cells. Followed by this, cells were incubated at 37°C in a tissue culture incubator for 30 min, 60 min, and 120 min. After the respective incubation period, cells were washed two times with HBSS and subsequently imaged on a wide-field epifluorescence microscope to record fluorescence intensity in DAR (G) and A647N (R) channels. The integrity of the *NOckout* inside cells can be compromised in endosomes or phagosomes due to the presence of DNAases in those

compartments. Potentially, DNAase can degrade dsDNA backbone of *NOckout* and A647N fluorophore of the *NOckout* could escape due to this degradation from the endosomal compartments to the cytoplasm. On the contrary, DAR attached to the DNA through a 10 kDa PEG spacer will retain in the endosomes even after DNA degradation due to its polymeric nature. Thus, a dramatic increase in G/R signal would indicate an active DNA degradation process due to the loss of A647N (R) signal. Our experiments with *NOckout* in cells are completed within 2 hours and we have not noticed any degradation of our probes with in this time period (SI Figure 12).

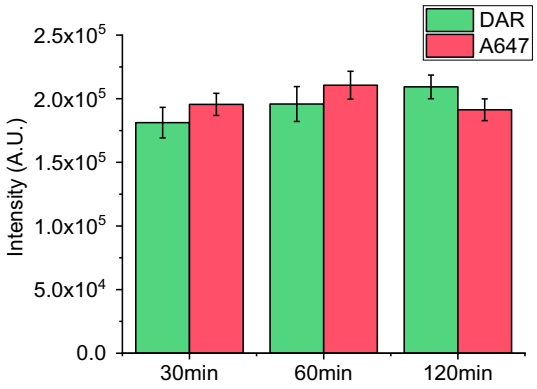

Supplementary Figure 12: Stability of *NOckout* in J774A.1 cells. Pre-turned on *NOckout* pulsed cells were incubated at 37°C and images were acquired in DAR (G) and A647N (R) channels. Whole cell intensities (n = 15 cells) in each channel is plotted at different time points. Error bar represents standard deviation from three independent replicates.

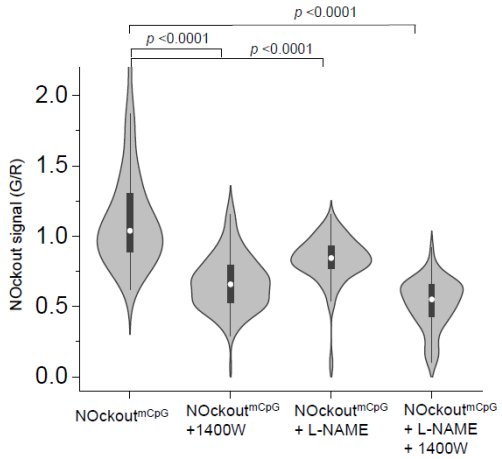

Supplementary Figure 13: Violin plot showing the distribution of G/R values of ~100 individual endosomes (from n=3 replicates) of J774A.1 cells treated with *NOckout*^{mCpG} in the presence of 1400W (100 μM, NOS2 inhibitor and L-NAME (2 mM, pan NOS inhibitor). White circle represents the median G/R value and black bar represents the distribution from 25%−75%.

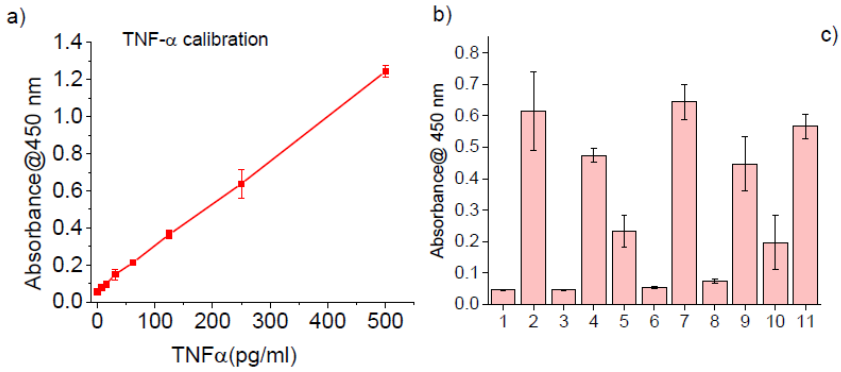

	Sample	TNFα (pg/ml)	Std.Dev
1	*Blank*	0.44	0.092
2	*mCpG*	237.29	96.01
3	*mGpC*	1.01	0.07
4	*iRNA*	176.45	17.06
5	*RNA*	72.07	32.22
6	*NOckout*	1.82	0.03
7	*NOckout^{mCpG}*	250.28	112.22
8	*NOckout^{mGpC}*	5.70	3.34
9	*NOckout^{iRNA}*	163.81	68.32
10	*NOckout^{fRNA}*	61.93	13.51
11	*LPS (350 ng/ml)*	233.22	32.26

Supplementary Figure 14: Quantification of TNF-α in J774A.1 cells. (a) Calibration curve generated for TNF-α using vendors kit. Error bars represents standard deviation from three independent experiments (b) Plot showing abosorbance at 450 nm for each samples. Error bar represents standard deviation from n = 3 experiments. (c) Table showing quantification of TNF-α for individual samples.

Precautions taken to avoid LPS-contamination of NOckout probes: For cellular and *in vivo* applications, we used commercially available, endotoxin-tested HBSS to anneal *NOckout* probes. After assembling each *NOckout* probe, its immunogenicity was checked by ELISA to detect TNF-α using ELISA. *NOckout* probes devoid of TLR-stimulating ligands showed negligible TNF-α production over the untreated sample (SI Fig.14), indicating that any potential sample contamination by ubiquitous endotoxins is negligible. For *in vivo* experiments, zebrafish larvae were bathed in sterile endotoxin-free HBSS (0.2 micron filtered) or E3-medium. Microinjection needles were prepared just prior to injection to minimize exposure of the needle tip to environmental endotoxins, thus minimizing potential sources of LPS contamination.

Intracellular localization of NOckout in J774A.1 cells: Co-localization studies were conducted to reveal the identity of the vesicular compartments in J774A.1 cells labeled with *NOckout*. We used different endosomal markers for early endosomes (EE), late endosomes (LE) and lysosomes (LY). TMR-conjugated transferrin, FITC-conjugated ovalbumin and TMR-dextran for marking EE, LE and LY respectively were used in previously published protocols[6]. *NOckout* showed significant co-localization with LE at 90 min, the time at which steady-state NO-measurements were performed (SI Figure 15). Immunofluorescence using anti-LAMP-1 (LY maker) antibodies in J774A.1 cell showed no co-localization of *NOckout* with LY (SI Fig 15b). From these experiments, we observe that *NOckout* reports NO primarily from LE.

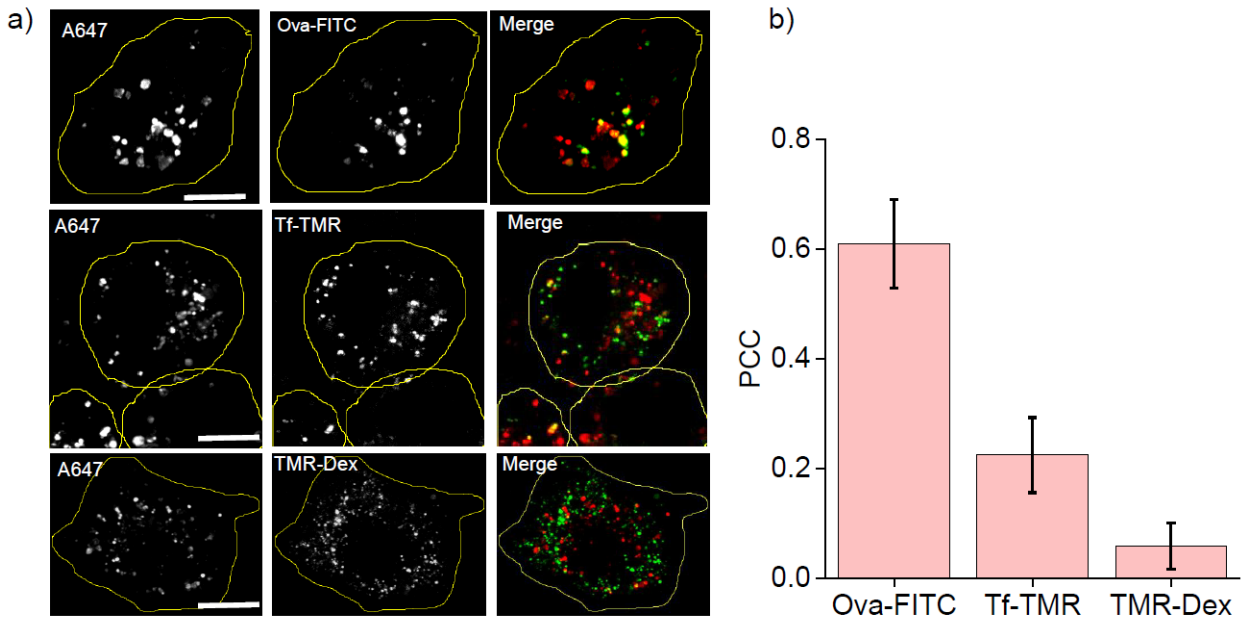

Supplementary Figure 15a: (a) Co-localization of *NOckout* with endosomal markers in J774A.1 cells. (b) Quantification showing Pearson Correlation Coefficient (PCC) for different endosomal markers. Error bar represents standard deviations from n=20 cells in each treatment. Scale bar = 10 μm.

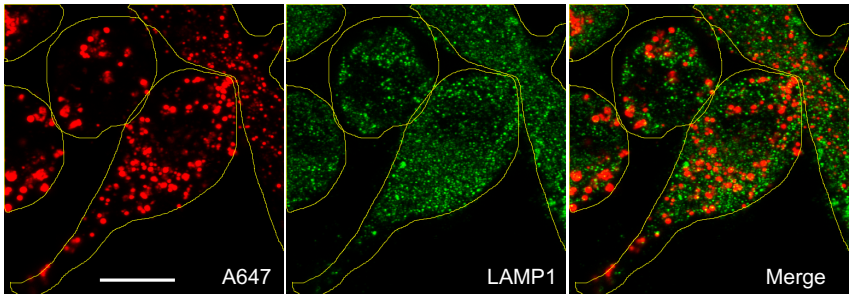

Supplementary Figure 15b: (a) Anti-colocalization of *NOckout* at 90 min with lysosomal marker LAMP1 in J774A.1 cells. *NOckout* was imaged in A647 (red) channel and LAMP1 was imaged using A488-labeled secondary antibody. Scale bar = 10 μm.

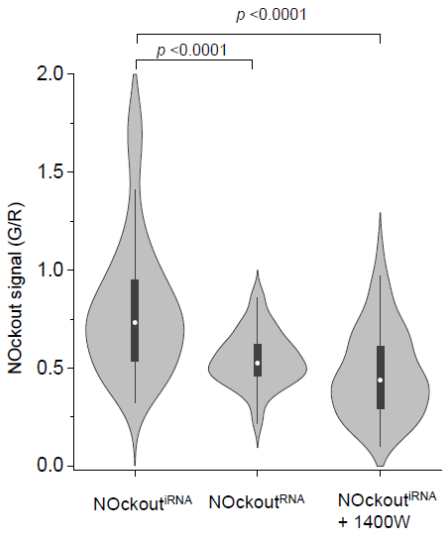

Supplementary Figure 16: Violin plot showing the distribution of G/R values of ~100 individual endosomes (from n = 3 replicates) of RAW264.7 cells treated with *NOckout*^{iRNA} and *NOckout*^{RNA} in the presence of 1400W (NOS2 inhibitor).White circle represents the median G/R value and black bar represents the distribution from 25%−75%.

Endosomal pH perturbation using Bafilomycin A$_1$: Bafilomycin A$_1$ (BAF) is a macrolide antibiotic that selectively inhibits the vacuolar type H^+-ATPase (V-ATPase) and prevents the acidification of endosomal organelles. It has been known from previous studies that TLR-mediated signaling is dependent on acidification of endosomal/lysosomal compartments[7,8]. We have added 200 nM of BAF one hour prior to and during the addition of *NOckout*^{mCpG} (500 nM, for 120 min) in primary mouse microglial cells. *NOckout*^{mCpG} signals in DAR (G) and A647N (R) channels were collected using the image settings described above. The G/R values for individual endosomes were calculated from corresponding ROI intensities in the G and R channel images. *NOckout*^{mCpG} incubated samples showed a high population of endosomes with a high G/R value compared to that of the (*NOckout*^{mCpG}+BAF) treated sample (SI Figure 13). About 70% of endosomes in *NOckout*^{mCpG} treated sample showed a G/R value ≥ 0.45 compared to only 50% observed in BAF treated sample (SI Figure 13). This result indicates that a perturbed TLR signaling due to the change in endosomal acidification leads to an aberrant NO production in those compartments.

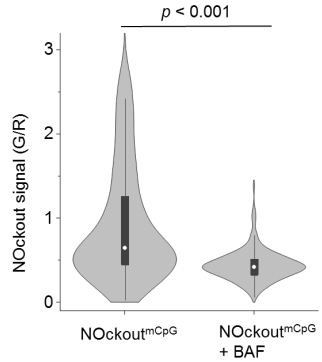

Supplementary Figure 17: Bafilomycin A1 treatment perturbs NO production in endosomes in microglia. (a) Distribution of *NOckout* signal from endosomes (n = 300 endosomes from 3 replicates) of primary microglial cells). White circle represents the median G/R value and black

bar represents the distribution from 25%−75%. P value is obtained by using Kruskal-Wallis statistical test.

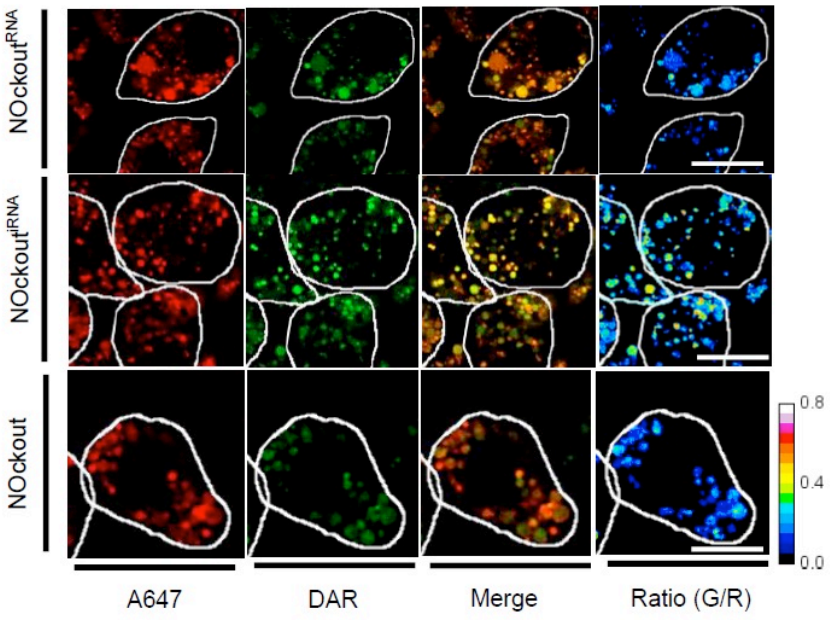

Supplementary Figure 18: Representative images of *NOckout*^{RNA} and *NOckout*^{iRNA} (500 nM each) pulsed samples from J774A.1 cells. Red represents fluorescent signal from A647N and green represents DAR signal. Ratio images in heatmap represents endosomal G/R values. Scale = 10 μm.

Protein homology modelling: We utilized SWISS-MODEL server in order to perform zTLR-7 homology modelling[9,10]. Fully automated workflow on the UniProt provided zTLR-7 sequence gave us following modelling results.

Model #	Template	Description	Query coverage	QMEAN*
1	5gmf.1.A	Macaca TLR-7	0.77	-2.23
2	3j0a.1.A	Human TLR-5	0.75	-8.82
3	2a0z.1.A	Human TLR-3	0.62	-6.93

*QMEAN is a composite scoring function, which is able to derive both global (i.e. for the entire structure), and local (i.e. per residue) error estimates based on one single model. Scores of -4.0 or below are an indication of models with low quality.

Model #1 shows the QMEAN value of -2.23, which depicts good global and local homology between, sequences as evident from Figure S21. Other TLRs like TLR-5 and TLR-3, which do give decent query coverage but do not show acceptable QMEAN values in homology modelling. Our homology modelling results suggest that zTLR-7 is similar to Macaca TLR-7 structurally and sequence wise (74% similarity, Figure S20 & 21).

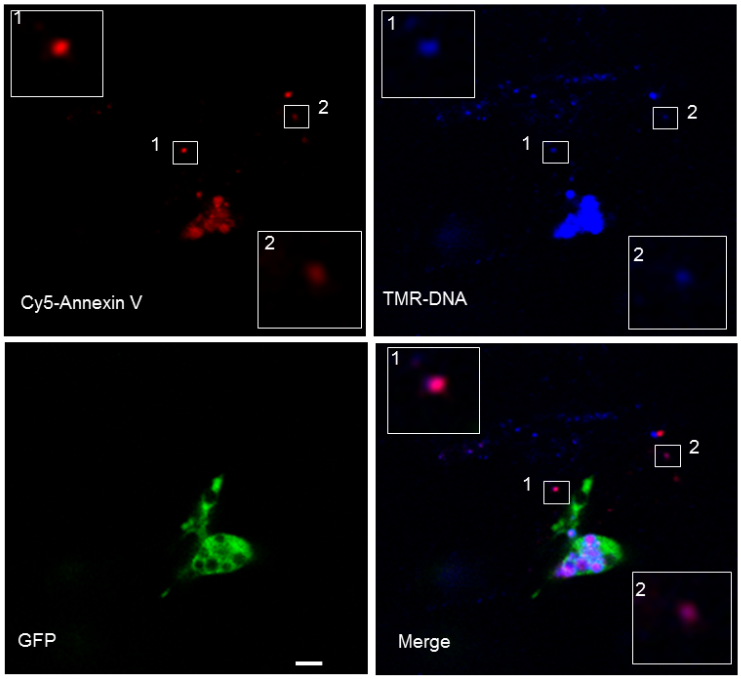

Supplementary Figure 19: Microinjected dsDNA^{TMR} (24-mer) (blue) co-localizes with apoptotic body (red) prior to its uptake by the microglial cells (green). Inset shows zoomed images of the co-localized puncta. Scale = 10 μM

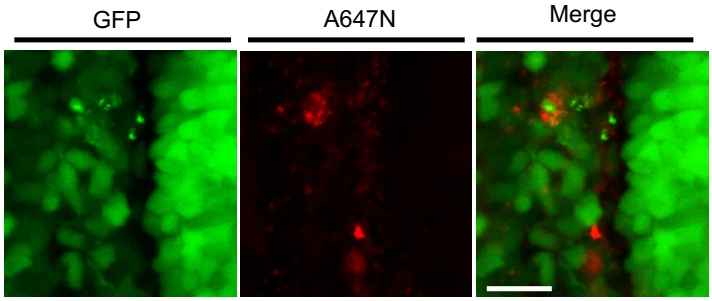

Supplementary Figure 20: Neurons do not uptake dsDNA^{A647} (24-mer) injected in the brain. Images of 3 dpf old (*Tg(Huc:Kaede)*) fish injected with dsDNA^{A647} (10 μM, 20 nL) recorded in the optic tectum area. Green represents *Kaede* emission from all the neurons (520 nm) and red represents fluorescence emission from dsDNA^{A647N}. Merged image indicates anti-colocalization of dsDNA with the neurons. Scale = 30 μm.

Zebrafish TLRs	Zebrafish PAMPs	Mammalian TLRs	Mammalian PAMPs
TLR1		TLR1	lipopeptides and peptidoglycan
TLR2	lipopeptides; Pam3CSk4	TLR2	lipoproteins, lipoteichoic acid
TLR3	dsRNA; Poly I:C	TLR3	dsRNA

TLR4a/b		TLR4	LPS or Mannan
TLR5a/b	flagellin	TLR5	flagellin
TLR7		TLR6	lipopeptide
TLR8a/b		TLR7	ssRNA
TLR9	CpG-ODNs	TLR8	ssRNA
TLR14		TLR9	CpG-ODNs
TLR18		TLR10	
TLR19		TLR13	rRNA
TLR20a			
TLR21	CpG-ODNs		
TLR22	dsRNA; Poly I:C		

Supplementary Table 2: Table summarizes all the TLR receptors discovered till date in zebrafish and mammals (human and mouse). Respective PAMPs for the zebrafish and mammalian TLRs are also shown.

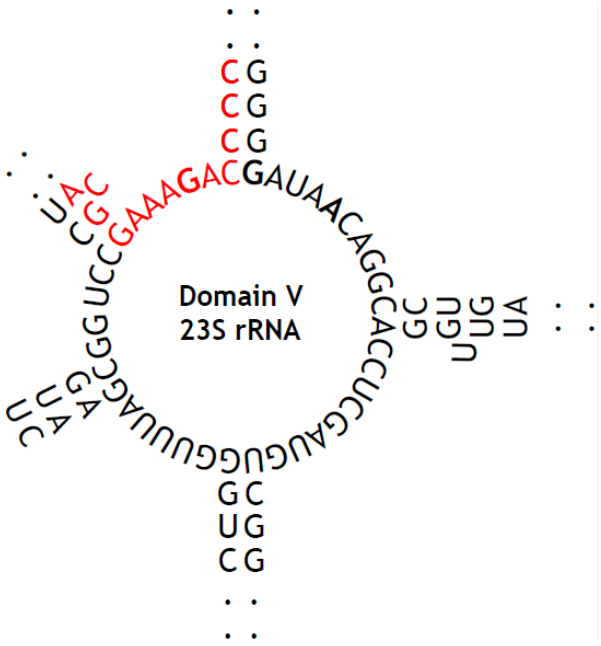

Supplementary Figure 21: Structure of the rRNA ribozyme (domain V) hosting the conserved immunogenic 13nt RNA sequence highlighted in red.

Species	23s rRNA sequence	Comments
S.Typhimurium	2095 ACGGAAAGACCCC 2107	Used to study innate immunity in zebrafish
M.Marinum	2260 AAAGACCCC 2268	Widely used as a model for studying innate immunity in zebrafish
M.Tuberculosis	2255AAAGACCCC2263	Tuberculosis model in zebrafish
M. Leprae	2277 AAAGACCCC 2285	Used to study innate immunity in zebrafish

Aeromonas hydrophila	2045ACGGAAAGACCCC2057	Aquatic bacterium that cause high mortality in zebrafish, NO/ROS production observed during infection
Edwardsiella tarda	2048ACGGAAAGACCCC2060	Natural pathogen of zebrafish. Induces robust NO production within 2h in Japanese flounder.
E. coli	2054ACGGAAAGACCCC2066	
Francisella philomiragia	2047ACGGAAAGACCCC2059	iNOS upregulation reported in zebrafish

Supplementary Table 3: Table shows bacterial species hosting the immunogenic 13nt rRNA sequence in their 23s rRNA. Aquatic pathogens such as *Aeromonas hydrophila* and *Edwardsiella tarda* (in bold) has 100% sequence conservation. *Mycobacterium* has partial sequence identity.

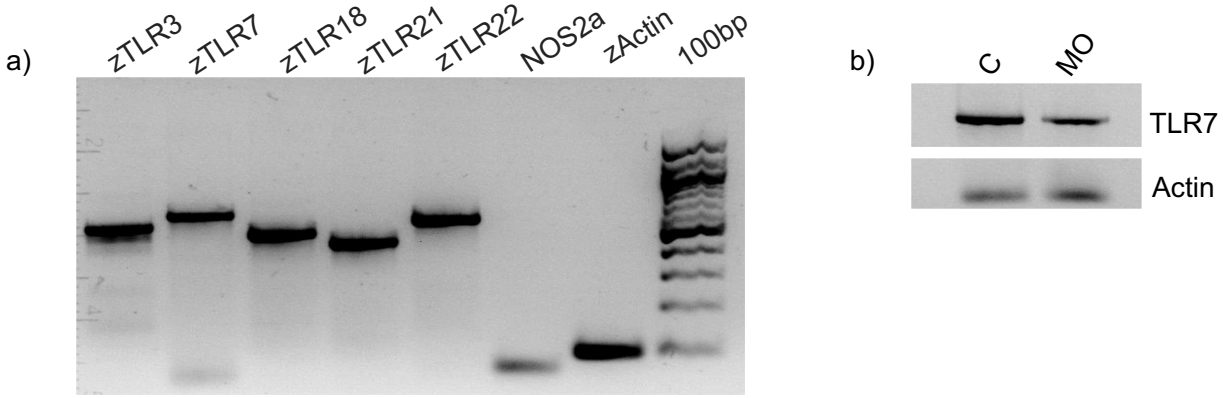

Supplementary Figure 22: (a) RT-PCR detection of mRNAs of zebrafish TLR (zTLR) receptors in 3dpf old larval zebrafish. (b) Validation of morpholino knockdown of zTLR7 in 3 dpf old fish. Actin mRNA is used as the loading control.

Morpholino Name	Sequence (5'-3')
TLR3	TCATTAGATCCATATTTTCCTTCCT
TLR7	TCATGGTCTTCTCAGTCATCTGAAA
TLR9	TCAAGGACACCATTGGTCCAAACAT
TLR18	AGTACCAGCGGAACAAGCATTTTCA
TLR22	GCTTTCTCTTGATTTCCTTTTCATT
NOS2a	ACAGTTTAAAAGTACCTTAGCCGCT[11]

Supplementary Table 4: Morpholino sequences employed in this study

Gene	Forward Primer (5'-3')	Reverse Primer (5'-3')
zTLR3	GGTACACTTCCAGGGATGGAGA	TTCTAGTTGACCTTGTTTGTAGAG
zTLR7	CTCTGTATTTTCCAAACCACTCTG	CCTGATCACAGAGTCTCCTGAAAG
zTLR9	GGGGAAGATGGCGCT TTCAG	CCA GAA GAG CGGCTG CACTC
zTLR18	TTTAGGTCAAGGGGTGGATTAC	CTACTATGTCGGCTGATTGTTCTC
zTLR21	GGAGAACAG TGGCGTCGCTTAC	GTTCTT TTG CACTGTTTGGATCAG

zTLR22	GTTTGCAGCAGTATTTTG GTCATC	GTTCTCTGATTTATGGCTGTCTTTG
zActin	CGAGCAGGAGATGGGAACC	CAACGGAAACGCTCATTGC

Supplementary Table 5: RT-PCR primer sequences used in this study.

Supplementary Figure 23: (a) Predicted zTLR7 (magenta) structure superimposed with the known crystal structure of ssRNA (orange) bound Rhesus macaque TLR7(cyan) (PDB:5GMF).

```
CLUSTAL O(1.2.4) multiple sequence alignment

sp|Q9NYK1|TLR7_HUMAN        MVFPMWTLKRQILILFNIILISKLLGARWFPKTLPCDVTLDVPKNHVIVDCTDKHLTEIP        60
tr|F1QY64|F1QY64_DANRE      -------MTEKTMIIF-ASFISLLVAAEWYPKSLKCDVSLASNGTEVSVDCTERSLTEVP        52
                                   :..: :*:*   :** *:.*.*:**:* ***:*    ..* ****:: ***:*

sp|Q9NYK1|TLR7_HUMAN        GGIPTNTTNLTLTINHIPDISPASFHRLDHLVEIDFRCNCVPIPLGSKNNMCIKRLQIKP        120
tr|F1QY64|F1QY64_DANRE      LGIPTNTTNLTLTINHIPHVMNNSFDNLHNITEIDLRCNCVPVKVGPKDRVCSQSVSIDN        112
                             ****************.:   **..*.::.***:******: :* *:.:* : :.*.

sp|Q9NYK1|TLR7_HUMAN        RSFSGLTYLKSLYLDGNQLLEIPQGLPPSLQLLSLEANNIFSIRKENLTELANIEILYLG        180
tr|F1QY64|F1QY64_DANRE      GTFWKLKNLKSLYLDGNQLSSIPKGLPANIVLLSLEINSIYSILQENLTELTNIRTLYLG        172
                             :*  *. ********** .**:*** .: ***** *.*:** :******:**. ****

sp|Q9NYK1|TLR7_HUMAN        QNCYYRNPCYVSYSIEKDAFLNLTKLKVLSLKDNNVTAVPTVLPSTLTELYLYNNMIAKI        240
tr|F1QY64|F1QY64_DANRE      QNCYFRNPCNQSYYIEKDAFMLLDKMTLLSLKSNNLSYIPNQLPSSLKELYLYNNNIEKI        232
                            ****:****  ** ******: * *:.:****.**:: :*. ***:*.******* * **

sp|Q9NYK1|TLR7_HUMAN        QEDDFNNLNQLQILDLSGNCPRCYNAPFPCAPCKNNSPLQIPVNAFDALTELKVLRLHSN        300
tr|F1QY64|F1QY64_DANRE      TENDFCNLTELEVLDLSGNCPRCYNAPFPCIPCPNNAPLQIHPNSFKTLRNLKTLRLHSN        292
                             *:** **.:*::**************** ** **:****  *:*.:* :**.******

sp|Q9NYK1|TLR7_HUMAN        SLQHVPPRWFKNINKLQELDLSQNFLAKEIGDAKFLHFLPSLIQLDLSFNFELQVYRASM        360
tr|F1QY64|F1QY64_DANRE      SLTNIPPEWFQSLADLTLLDLSSNFLAKEITCTSFPSLLPKLEELDLSFNYELQVYPASL        352
                            ** ::**.**:.: .*  ****.*******  :.*  :**.* :******:***** **:

sp|Q9NYK1|TLR7_HUMAN        NLSQAFSSLKSLKILRIRGYVFKELKSFNLSPLHNLQNLEVLDLGTNFIKIANLSMFKQF        420
tr|F1QY64|F1QY64_DANRE      SLSESFSQLKSLRVLRIRGYVFQELKLQDIQPLTNLTYLEFLDLGTNFIKIAQLSILKNL        412
                            .**::**.****::********:***  ::.** **  **.**********:**::*::

sp|Q9NYK1|TLR7_HUMAN        KRLKVIDLSVNKISPSGDSS------EVGFCSNARTSVESYEPQVLEQLHYFRYDKYARS        474
tr|F1QY64|F1QY64_DANRE      KNFKIINLSDNKISVPSEGEFSFSNHREAYYGSPMSQGAQYHNGEVKDMHYFLYDEFARS        472
                            *.:*:*:** ****  .:..      . .: ..  :.  .*.   ::::*** **::***
```

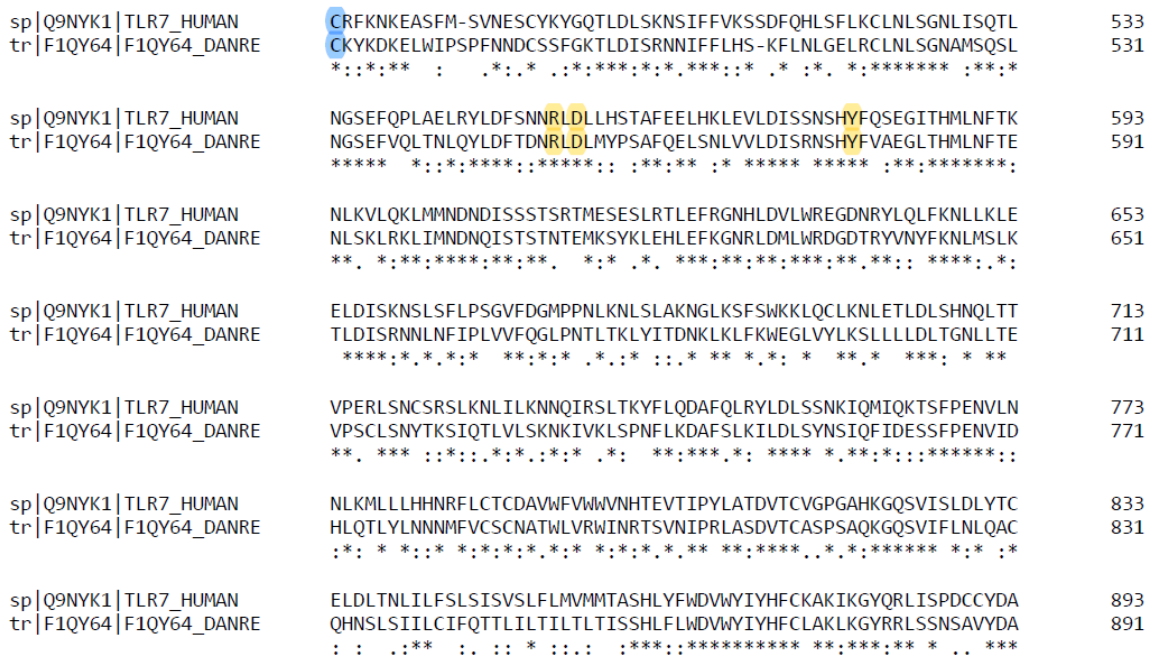

Supplementary Figure 24: Clustal Omega multiple sequence alignment showing the similarity between zTLR7 (Uniprot ID: F1QY64) and human TLR7 (Uniprot ID: Q9NYK1) amino acid sequences. Highlighted residues in blue are critical for ssRNA binding and in yellow are residues important in NF−κB activation in HEK293T cells[12,13]. Residues important in both ssRNA binding and NF−κB activation are either conserved or show conservative mutations in the zebrafish counterpart.

Supplementary Movie SM1: Movie showing the dynamics of microglia in the whole brain of 3dpf old *Tg(mpeg:EGFP)* zebrafish. Microglia is seen as the highly dynamic GFP expressing cells (green).

Supplementary Movie SM2: Movie showing the phagocytosis of injected *NOckout*^{UN} (red) in the optic tectum of *Tg(mpeg:EGFP)* zebrafish recorded for an interval of 15 minutes. Active phagocytosis events showing *NOckout*^{UN} (red) uptake by microglia can be seen in the movie.

Supplementary Movie SM3: 3D rendering of phagocytosis of *NOckout*^{UN} (red) using Imaris software. Phagosomal localization of the *NOckout*^{UN} (red) in microglia (green) is evident in the movie.

References

1. Minter, M. R. *et al.* Deletion of the type-1 interferon receptor in APPSWE/PS1ΔE9 mice preserves cognitive function and alters glial phenotype. *Acta Neuropathol. Commun.* **4,** 72 (2016).
2. Saura, J., Tusell, J. M. & Serratosa, J. High-yield isolation of murine microglia by mild trypsinization. *Glia* **44,** 183–189 (2003).

3. Kuppusamy, P. & Zweier, J. L. Characterization of free radical generation by xanthine oxidase. Evidence for hydroxyl radical generation. *J. Biol. Chem.* **264,** 9880–9884 (1989).
4. Berlato, C. *et al.* Involvement of suppressor of cytokine signaling-3 as a mediator of the inhibitory effects of IL-10 on lipopolysaccharide-induced macrophage activation. *J. Immunol.* **168,** 6404–6411 (2002).
5. Park, H. S. *et al.* Cutting edge: direct interaction of TLR4 with NAD(P)H oxidase 4 isozyme is essential for lipopolysaccharide-induced production of reactive oxygen species and activation of NF-kappa B. *J. Immunol.* **173,** 3589–3593 (2004).
6. Prakash, V. *et al.* Quantitative maps of endosomal DNA processing by single molecule counting. *Angew. Chem. Int. Ed. Engl.* **58,** 3073–3076 (2019).
7. Häcker, H. *et al.* CpG-DNA-specific activation of antigen-presenting cells requires stress kinase activity and is preceded by non-specific endocytosis and endosomal maturation. *EMBO J.* **17,** 6230–6240 (1998).
8. Ahmad-Nejad, P. *et al.* Bacterial CpG-DNA and lipopolysaccharides activate Toll-like receptors at distinct cellular compartments. *Eur. J. Immunol.* **32,** 1958–1968 (2002).
9. Waterhouse, A. *et al.* SWISS-MODEL: homology modelling of protein structures and complexes. *Nucleic Acids Res.* **46,** W296–W303 (2018).
10. Guex, N., Peitsch, M. C. & Schwede, T. Automated comparative protein structure modeling with SWISS-MODEL and Swiss-PdbViewer: a historical perspective. *Electrophoresis* **30,** S162-73 (2009).
11. Hall, C. J. *et al.* Infection-responsive expansion of the hematopoietic stem and progenitor cell compartment in zebrafish is dependent upon inducible nitric oxide. *Cell Stem Cell* **10,** 198–209 (2012).
12. Zhang, Z. *et al.* Structural Analysis Reveals that Toll-like Receptor 7 Is a Dual Receptor for Guanosine and Single-Stranded RNA. *Immunity* **45,** 737–748 (2016).
13. Colak, E. *et al.* RNA and imidazoquinolines are sensed by distinct TLR7/8 ectodomain sites resulting in functionally disparate signaling events. *J. Immunol.* **192,** 5963–5973 (2014).